Available online at www.sciencedirect.com
ScienceDirect
Polymer 49 (2008) 1934–1942
polymer
www.elsevier.com/locate/polymer

Micromechanical behaviour of particulate polymer nanocomposites

George I. Anthoulis, Evagelia Kontou*

School of Applied Mathematical and Physical Sciences, Section of Mechanics, National Technical University of Athens, 5 Heroes of Polytechnion, GR-15773 Athens, Greece

Received 1 November 2007; received in revised form 7 February 2008; accepted 7 February 2008
Available online 12 February 2008

Abstract

A large number of works deal with material synthesis and characterization of polymer nanocomposites due to their improved thermo-mechanical properties, but the fundamental mechanisms for mechanical property enhancement are not yet completely defined. In particular, a special class of polymer/organoclay nanocomposites has been observed to exhibit an impressive improvement in different types of properties, physical and chemical ones. In the present work, a model is presented and applied to formulate the elastoplastic response of epoxy/clay nanocomposites, experimentally tested elsewhere. The model based on Mori–Tanaka theory, for the estimation of the elastic stiffness tensor for composite materials, is combined with the self-consistent model of Budiansky and Wu, valid for crystal plasticity. Then the macroscopic plastic response of the heterogeneous material is linked with the microstructural parameters, i.e., the plastic behaviour of the effective particle. The model was proved to successfully describe the tensile response of the epoxy/clay nanocomposites with varying clay weight fraction.

Keywords: Polycyanurate; Nanoclay; Micromechanical

1. Introduction

Over the last years, polymer/clay nanocomposites have attracted great scientific and industrial interest, because of the remarkable improvement seen in materials' properties, not met by virgin polymer or conventional micro- and macro-composites. A polymer nanocomposite contains particles (or fillers) dispersed in a polymer matrix, where one or more of the dimensions of the particle is on the nanometer lengthscale [1]. One particular class of polymer nanocomposites that has received special attention is that of organic/clay ones [2]. The outstanding improvement obtained in many properties such as tensile modulus, strength and toughness at both low and high temperatures, increment of transition temperatures, flammability resistance, ablation and moisture/gas barrier performance [1–6], makes polymer/clay nanocomposites the materials of choice in several structural and functional applications. In addition, polymer/clay nanocomposites are lighter in weight compared to the conventionally filled polymers thus achieving a higher degree of stiffness and strength with far less high density inorganic materials [7] and they retain the optical transparency of the parent polymer because the size of the particles is less than the wave length of the visible spectrum [8].

The enhancement in mechanical properties observed in nanocomposites has led to the development of various models [9–13] that attempt to predict the behaviour of these materials from a mechanical or physical viewpoint. For instance, several models have been proposed for the prediction of the effective moduli of unidirectional nanocomposites with dispersed and parallel flake-like inclusions (e.g. Refs. [9,10]), but the fundamental mechanism for mechanical enhancement of polymer nanocomposites is not yet completely defined [11–13]. For conventional polymer/fiber composites, where the filler dimensions are in the range of tens of microns or larger, continuum mechanics models are applied with considerable success. In organic/clay nanocomposites, these models need to be properly modified owing to the major differences in behaviour between conventional and nanostructured materials related with the much larger surface area per unit volume existing

* Corresponding author. Tel.: +30 210 7721219; fax: +30 210 7721302.
E-mail address: ekontou@central.ntua.gr (E. Kontou).

0032-3861/$ - see front matter © 2008 Elsevier Ltd. All rights reserved.
doi:10.1016/j.polymer.2008.02.010

in the latter. As emphasized by Brune and Bicerano [14], the concepts of matrix or filler, as known in conventional particulate composites, attain a different meaning in the case of polymer/clay nanocomposites. The reason for that is the hierarchical nanometer lengthscale morphology of the particle structure and the surrounding matrix.

In micromechanics modelling, nanoparticles are often considered to consist of layers ~1 nm in thickness and lateral dimensions from 300 Å to several microns, depending on the particular silicate. Stacking of these layers leads to a regular van der Waals gap between them so-called *interlayer* or *gallery*. The clay particles or their layers are incorporated into the polymer matrix by different ways, and therefore, polymer/clay composites can be divided into four categories [15] depending on clay content, degree of clay layer separation and distribution in the composite: conventional miscible composite, where the clay particles retain their original state of aggregated layers with no insertion of polymer matrix between them; intercalated composite, where extended polymer chains are inserted into the clay structure between the layers forming a well ordered multilayer with alternating polymer/inorganic domains and expanding the interlayer spacing by a few nanometers; exfoliated composite, where the 1 nm thick clay layers are uniformly dispersed in a continuous polymer matrix and segregated from one another by average distances that depend on clay loading; partially intercalated and exfoliated composite where the exfoliated layers and intercalated particles are randomly distributed into the matrix. An enhanced thermo-mechanical behaviour characterizes the polymer/nanoclay composites with either intercalated or exfoliated layers. Moreover, the exfoliated nanocomposites have better thermo-mechanical properties than the intercalated ones for the same clay content [15].

In the present paper, a micromechanics model based on Eshelby's eigenstrain idea [16], Mori–Tanaka's back stress analysis [17], and Chen and Cheng's model [18] initially proposed to determine the elastic stiffness tensor of polymer nanocomposites is combined with the self-consistent model of Budiansky and Wu [19] for plastic deformation to predict the elastoplastic behaviour of particulate composites. Taya and Chou's model [20] for the calculation of the longitudinal modulus of hybrid composites is used to estimate appropriate values for model parameters. Following this procedure, the macroscopic properties of heterogeneous materials are linked with their microstructural parameters. Constitutive laws for plastic deformation within the frame of Rubin's analysis [21,22] are written for both material structures, i.e., matrix and inclusions. The present model analytically presented in a previous publication [23] has been successfully applied on conventional composites as well as on polymers reinforced with silica nanoparticles. In this work, in order to account for the inherently discrete nanoclay structure, the concept of the 'effective particle' initially presented for separate clay sheets, is extended to involve the case of a nanosized particle or agglomerate surrounded by a percentage of matrix attached to it, that possesses different properties with respect to that of the matrix. Through this procedure, the coexistence of partial intercalation and exfoliation, the mechanical behaviour of nanoparticles, as well as the proper conversion of filler weight fraction to particle volume fraction are taken into account, providing a better understanding of the relationship between nanoclay content and structure and final nanocomposite properties. This concept is then satisfactorily applied on tensile results for epoxy/clay nanocomposites for different concentrations of clay, performed elsewhere.

2. Micromechanical models

In their work, Taya and Chou [20] starting from the concept of the eigenstrain idea of Eshelby [16] and based on previous works of Mori and Tanaka [17] and Taya and Mura [25] who considered the interaction among inclusions, introduced the idea of a back stress and extended Mori–Tanaka's theory to three-phased composites with two different kinds of inhomogeneities. The overall stiffness assessment of these materials was then possible. Taya and Chou's model was also valid when reduced in the case of particulate reinforcement. For the calculation of the longitudinal modulus they used the equivalence of the strain energies and obtained the following equation:

$$\frac{E_{11}}{E_{\mathrm{m}}} = \frac{1}{1+h} \tag{1}$$

where E_{11} is the longitudinal modulus of the composite material and E_{m} the matrix elastic modulus. The quantity h is a

$$\begin{aligned}
S_{11} &= S_{22} = \frac{3}{8(1-\nu)}\frac{t_1^2}{(t_1^2-1)} + \frac{1}{4(1-\nu)}\left[1-2\nu-\frac{9}{4(t_1^2-1)}\right]g_1 \\
S_{33} &= \frac{1}{2(1-\nu)}\left[1-2\nu+\frac{3t_1^2-1}{t_1^2-1}-\left\{1-2\nu+\frac{3t_1^2}{t_1^2-1}\right\}g_1\right] \\
S_{12} &= S_{21} = \frac{1}{4(1-\nu)}\left[\frac{t_1^2}{2(t_1^2-1)}-(1-2\nu)-\frac{3}{4(t_1^2-1)}g_1\right] \\
S_{13} &= S_{23} = -\frac{1}{2(1-\nu)}\frac{t_1^2}{(t_1^2-1)} + \frac{1}{4(1-\nu)}\left[\frac{3t_1^2}{t_1^2-1}-(1-2\nu)\right]g_1 \\
S_{31} &= S_{32} = -\frac{1}{2(1-\nu)}\left[1-2\nu+\frac{1}{t_1^2-1}\right] + \frac{1}{2(1-\nu)}\left[1-2\nu+\frac{3}{2(t_1^2-1)}\right]g_1
\end{aligned} \tag{2}$$

function of filler volume fraction, the elastic constants of matrix and filler as well as the components of the Eshelby tensor. The Eshelby tensor components for prolate inclusions were applied, given by Eq. (3):where ν is the Poisson ratio of the matrix, t_1 is the aspect ratio of the particle and the quantity g_1 is given by the expression [20]:

$$g_1 = \frac{t_1}{(t_1^2-1)^{3/2}}\left[t_1\left(t_1^2-1\right)^{1/2} - \cos h^{-1} t_1\right] \tag{3}$$

3. Clay morphology parameters

The improvement of nanocomposites mechanical properties has been studied by applying models that take into account the existence of both intercalation and exfoliation. This analysis provides a better understanding of the material's morphology [15] and will also be supported by the results of various experimental techniques.

The materials utilized in this study were developed in the works of Luo and Daniel [15] and Daniel et al. [24] and will be referred to as series A and series B specimens, respectively. In both cases, the reinforcing phase was a commercial grade of montmorillonite, Cloisite 30B from Southern Clay Products, USA. Clay particles were disk-like stacks of thin silicate layers, 1 nm thick with a diameter ranging from 100 nm to several micrometers. The specific gravity of the clay particles (stacks) is 1.98 g/cm^3 and the d-spacing is 1.85 nm. The modulus of an individual layer (platelet or flake) is 170–180 GPa and its specific gravity is 2.5 g/cm^3. Two epoxy systems were used as matrices. In series A, a Dow epoxy resin (DER 331) modified with DER 732 and cured with Dow epoxy hardener (DEH 24), and in series B, a three component epoxy system (Ciba-Geigy GY 6010 unmodified epoxy, HY 917 hardener and DY070 accelerator). In series A, measurements were carried out for pure matrix and a nanocomposite with 5% per weight (wt%) concentration of clay, whereas in series B, tests concerned the neat matrix and nanocomposites with 2.5, 5 and 10 wt% organoclay loading. The detailed procedure of preparation and processing of these materials, in order to obtain well-exfoliated structures highly oriented and randomly distributed in the matrix is provided in the corresponding Refs. [15,24].

The quality of clay dispersion and structure of nanocomposites was assessed by transmission electron microscopy (TEM) and X-ray diffraction (XRD). Mechanical properties of epoxy/clay nanocomposite specimens were examined by monotonic uniaxial tension tests. These tests were conducted at different strain rates; 1.7×10^{-4} s^{-1} for series A and 1.7×10^{-3} s^{-1} for series B.

Before the presentation of the proposed model, it is imperative to establish the concept of the 'effective particle' [26]. Let us start from the conventional miscible composite where the polymer is unable to penetrate in the space between the clay layers. In this case, due to the absence of polymer–matrix interplay, the particle volume fraction can be calculated from the weight fraction through the equation:

$$f_p = \frac{W_p/\rho_p}{W_p/\rho_p + (1-W_p)/\rho_m} \tag{4}$$

where ρ_p and ρ_m are the clay particle and matrix densities correspondingly, and W_p is the particle weight fraction. However, in an intercalated nanocomposite, a significant number of polymer chains are inserted in the galleries and the interlayer spacing is correspondingly expanded, that is, the conversion of filler weight fraction to particle volume fraction can no longer be given by Eq. (4), because the hierarchical morphology of the particle is intrinsically different, owing to changes caused by the intercalated nanolayers and the surrounding matrix. Our scope in this section is the proper mapping of the characteristic clay structural parameters to micromechanical model parameters. Structural parameters directly related to processing include the clay weight fraction W_c, the clay atomic structure, the silicate interlayer spacing $d_{(001)}$ and the average number of silicate layers per clay stack N. Model parameters include the particle volume fraction f_p, the particle aspect ratio L/t (L is the length and t the thickness of the dispersed clay particle) and the ratio E_p/E_m of particle to matrix stiffness. In combination with model parameters determined from experiments such as XRD or TEM, this concept will be then applied to simulate the tensile behaviour of two epoxy/nanoclay systems.

In the case of an intercalated nanocomposite, where the particle contains silicate sheets as well as interlayer galleries, the particle weight fraction W_p differs from clay weight fraction W_c. These quantities are related in terms of the following equation [26]:

$$\frac{W_p}{W_c} = \frac{\rho_p V_p}{\rho_{silicate} V_{silicate}} = \left(\frac{\rho_p}{\rho_{silicate}}\right)\Big/\left(\frac{V_{silicate}}{V_p}\right) = \frac{\rho_p}{\rho_{silicate}}\frac{1}{\chi} = \alpha \tag{5}$$

where $\chi = V_{silicate}/V_p$ is the volume fraction of silicate in the effective particle and $\rho_{silicate}$ is the density of the silicate sheet. The latter is calculated by implementing the parameters of the montmorillonite lattice [26,27]:

$$\rho_{silicate} = \rho_{lattice} = \frac{M_0}{A_0 d_s} = \frac{2.44}{d_s}\,\text{nm g/cm}^3 \tag{6}$$

where $M_0 = 720$ g/mol is the molecular weight and $A_0 = a_0 b_0 = 0.49$ nm^2 the planar area of the lattice, respectively. In the latter equation, a_0 and b_0 represent the planar dimensions of the lattice, being equal to 0.53 and 0.92 nm [27], correspondingly. From Eq. (5) we have $W_p = \alpha W_c$, so Eq. (4) becomes:

$$f_p = \frac{W_c/\rho_p}{W_c/\rho_p + (\frac{1}{\alpha} - W_c)/\rho_m} \tag{7}$$

and assuming W_c small we obtain:

$$f_p \simeq \left(\frac{\rho_m}{\rho_{silicate}}\frac{1}{\chi}\right) W_c \tag{8}$$

On the other hand, χ is given by:

$$\chi = \frac{Nd_s}{(N-1)d_{(001)} + d_s} \tag{9}$$

where d_s is the silicate layer thickness. Furthermore, taking advantage of the equivalence of the effective particle with the multilayer stack [26], since they possess the same mechanical properties, the effective particle aspect ratio L/t can be given by the equation:

$$\frac{L}{t} = \frac{L}{(N-1)d_{(001)} + d_s} \tag{10}$$

Combining Eqs. (6), (8) and (9) and assuming $\rho_m = 1.16$ g/cm^3 (the mass density of epoxy matrix [28]), we obtain the following equation relating the conversion ratio f_p/W_c with N and the interlayer swelling $d_{(001)}/d_s$:

$$f_p/W_c = \frac{0.475 d_s}{\chi}\,\mathrm{nm}^{-1} = \frac{0.665\left((N-1)d_{(001)}/d_s + 1\right)}{N}\,\mathrm{nm}^{-1} \tag{11}$$

The only unknown parameters at this point are the silicate layer thickness and the effective particle modulus. As regards the former, we refer to the work by Manevitch and Rutledge [27]. There it was found with the help of molecular dynamics (MD) simulation that the stiffness of a single silicate sheet $E_{silicate}d_s$ is varied between 246 and 258 N/m. Hence, with the modulus of the single clay nanolayer $E_{silicate} = 176$ GPa [15], the layer thickness d_s is calculated to be 1.4 nm. With respect to the latter, as emphasized by Sheng et al. [26], the intercalated clay can be treated as a homogeneous isotropic particle under the assumptions of well aligned particles and axial loading.

Hence, in the following, we assume that the effective particle modulus E_p is analogous to the number of silicate sheets per particle thickness [26]:

$$E_p = \frac{Nd_s}{t}E_{silicate} \tag{12}$$

As was mentioned above, in the present analysis the effective particles are considered to have the shape of prolate inclusions. Hence, according to Eqs. (2) and (10), parameters such as the number of silicate layers, silicate layer length and thickness, and interlayer spacing N, L, d_s and $d_{(001)}$, respectively, are now included in the analysis and are required quantities to compute the longitudinal modulus of the composite, E_{11}. The effect of the clay structural parameters on E_{11}/E_m (E_m is the matrix modulus taken equal to 2.05 GPa [15]) for a clay concentration of 0–10 wt% was studied in terms of Eq. (1), and is analytically presented in Fig. 1. For the analysis, the interlayer spacing is fixed at 4.8 nm, based on the best estimates of TEM micrographs [15]. In this figure, the normalized modulus E_{11}/E_m is plotted against clay concentration for two specific values of L, with N ranging from 1 to 5, i.e., from completely exfoliated to well ordered intercalated nanocomposite. It is clearly observed that for fixed L, the ratio E_{11}/E_m sees

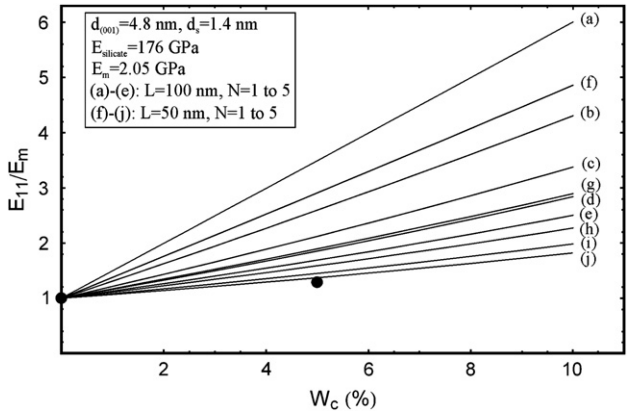

Fig. 1. Effect of clay structural parameters (N, L) on the macroscopic modulus, predicted by the Taya–Chou model [20] (Eq. (1)), at a fixed value of the interlayer spacing $d_{(001)}$. Model parameters used are indicated on the graph; the remaining ones are calculated from Eqs. (10)–(12). Closed circles: experimental ratios E_{11}/E_m calculated from the slope of the corresponding stress–strain curves in the elastic region (series A tests [15]); pure matrix (0 wt%) and nanocomposite (5 wt%).

an appreciable reduction as N increases, demonstrating the detrimental effect of intercalation versus exfoliation with regard to stiffness enhancement. Furthermore, the stiffness is also decreased with decreasing silicate layer length, emphasizing the importance of a high aspect ratio when a high stiffness is desired. Also included in Fig. 1 are the experimental ratios E_{11}/E_m 1 and 1.29 of the epoxy/clay nanocomposites of 0 and 5 wt%, respectively, calculated from the slope of the stress–strain curve in the elastic region [15], to give a better idea of the parametric dependence of nanocomposite stiffness. It is observed that the case $N = 5$ and $L = 50$ nm is in a satisfactory agreement with the experimental points. Consequently, the parameters chosen for the analysis for series A are: $N = 5$, $L = 50$ nm, $d_{(001)}$=4.8 nm, $d_s = 1.4$ nm, $E_p = 59.8$ GPa (from Eq. (12)). Substituting $W_c = 5$ wt% in Eq. (11) yields the effective particle volume fraction $f_p = 0.0978$ or 9.78 vol%.

In series B, the extent of nanolayer expansion was quantified by low-angle XRD measurements [24]. For the 10 wt% sample $d_{(001)}$ was detected at 4.57 nm, while for the sample with 2.5% clay loading, the XRD pattern did not reveal any clear peak, which was attributed to the low clay content resulting in small number of intercalated clusters. Samples with 5 wt% montmorillonite were not subjected to XRD analysis. Hence, in order to get appropriate values for the remaining unknown model parameters N and $d_{(001)}$, we examined the effect of their variation on the normalized composite modulus E_{11}/E_m. In Fig. 2 we compare the experimental ratios 1, 1.22, 1.37 and 1.62 for clay concentrations 0, 2.5, 5 and 10 wt%, respectively, with predictions of the final composite modulus calculated from Eq. (1). To simplify our calculations, we assume $L = 50$ nm which is reasonable based on Fig. 1 (in Fig. 1, all curves generated using $L = 100$ nm displayed a significant deviation from the experimental points). As it is evident from Fig. 2, $d_{(001)}$ variation has a minor impact on modulus, provided that the other parameters remain constant (see curves (2)–(4)), especially for clay concentrations

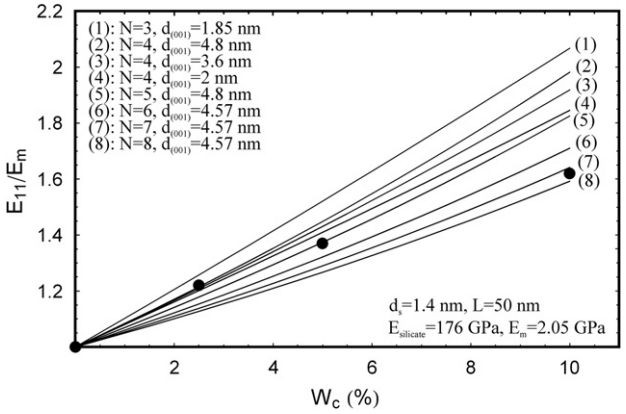

Fig. 2. Effect of N and $d_{(001)}$ on the macroscopic modulus, predicted by the Taya–Chou model [20] (Eq. (1)), at a fixed value of L. Model parameters used are indicated on the graph; the remaining ones are calculated from Eqs. (10)–(12). Closed circles: experimental ratios E_{11}/E_m calculated from the slope of the corresponding stress–strain curves in the elastic region (series B tests [24]); pure matrix (0 wt%) and nanocomposites (2.5, 5 and 10 wt%).

<2.5 wt%. That is, for clay loading 2.5 wt% where XRD showed no characteristic peak, $d_{(001)}$ can admit any value between 2 and 5 nm [15], while for $N=4$ there is a satisfactory agreement between the theoretical curves and the experimental ratio. At this point, we will assume that $d_{(001)}$ equals 2.4 nm, as it will be explained in Section 6. On the contrary, increasing N resulted in a considerable diminution in modulus. Referring back to Fig. 2, it is observed that for the 5 wt% sample, curve (5) (i.e. $N=5$ and $d_{(001)}$=4.8 nm) gives an adequate prediction, while for the 10 wt% sample this is the case for curve (7), i.e., for $N=7$ and $d_{(001)}$=4.57 nm. Substitution of the respective parameters in Eqs. (11) and (12), yields $f_p=0.0255$, 0.0978 and 0.1955 and $E_p=114.6$, 59.8 and 59.84 GPa for weight fractions 2.5, 5 and 10 wt% correspondingly.

In summary, based on the foregoing analysis, the parameters chosen for the calculation of the stiffness tensor, the components of the Eshelby tensor, as well as for the simulation of the tensile stress–strain results by the proposed model are listed in Table 1. The observation that upon addition of a relatively large amount of clay (10 wt%), the average number of silicate layers per clay stack, N, is considerably increased from 4 or 5 for lower concentrations to 7, suggests an enhanced degree of formation of intercalated nanoclusters.

Table 1
Characteristic clay structural and model parameters for the materials under study

Material (wt%)	L (nm)	d_s (nm)	$d_{(001)}$ (nm)	N	χ[a]	E_p (GPa)[b]	f_p[c]
Series A							
5	50	1.4	4.8	5	0.34	59.8	0.0978
Series B							
2.5	50	1.4	2.4	4	0.65	114.6	0.0255
5	50	1.4	4.8	5	0.34	59.8	0.0978
10	50	1.4	4.57	7	0.34	59.84	0.1955

[a] Calculated from Eq. (9).
[b] Calculated from Eq. (12).
[c] Calculated from Eq. (11).

4. Micromechanics model

The overall stiffness tensor of the nanocomposite materials has been calculated, assuming that they are composed of a continuous isotropic matrix and discrete isotropic inclusions. The estimation of the stiffness tensor follows previous works by Taya and Chou [20], and Chen and Cheng [18]. Their works are based on the results of Eshelby [16] and Mori–Tanaka [17]. Chen et al. have extensively studied the effective elastic moduli of planar orientation distribution and transversely isotropic distribution of fibers. The interaction among fibers at different orientations was included in their analysis by adopting the mean stress concept of Mori and Tanaka [17] together with the eigenstrain idea of Eshelby [16]. Extending this analysis, they have calculated the effective moduli tensor $\mathbf{C}^*$ for spherical particles acting as reinforcing agents, which is given by the equation:

$$\mathbf{C}^* = \mathbf{C}_m \cdot \left[\mathbf{I} + f_p \mathbf{B} \cdot \left(\mathbf{I} + f_p \mathbf{E}\right)^{-1}\right] \tag{13}$$

where f_p is the effective particle volume fraction, $\mathbf{C}_m$ the matrix stiffness tensor, $\mathbf{I}$ is the identity tensor, and

$$\begin{aligned} \mathbf{B} &= \mathbf{A} \cdot \mathbf{T} \\ \mathbf{A} &= \mathbf{I} - \mathbf{C}_m^{-1} \cdot \mathbf{C}_f \\ \mathbf{T} &= \left(\mathbf{I} + \mathbf{S} \cdot \mathbf{C}_m^{-1} \cdot \mathbf{C}_f - \mathbf{S}\right)^{-1} \\ \mathbf{E} &= (\mathbf{S} - \mathbf{I}) \cdot \mathbf{A} \cdot \mathbf{T} \end{aligned} \tag{14}$$

where $\mathbf{S}$ is the Eshelby tensor, taken here for prolate inclusions, with its components shown in Eq. (2). The combination of Eshelby's equivalent inclusion method and back stress analysis of Mori and Tanaka, which take into account the interactions among inhomogeneities becomes necessary when the volume fraction becomes large or as in the case of nanosized fillers the surface area becomes high.

The elastoplastic behaviour of the nanocomposites will be analyzed by combining the above-presented model with the self-consistent model of Kroner, Budiansky and Wu [19]. Budiansky and Wu proposed a self-consistent model that relates strain and stresses within the single crystal grains to the overall strain and stress. In their model, the interaction of a single crystal grain with the surrounding materials of the polycrystal was approximated by a sphere embedded in a homogeneous polycrystal matrix or aggregate. In the present work it is assumed that both grain and aggregate are elastically isotropic, while they are described by different elastic stiffness tensors $\mathbf{C}_f$ and $\mathbf{C}_m$ correspondingly. Since the size of a single crystal (or inclusion) is very small, the homogeneous aggregate or matrix is considered to be infinitely extended. The aggregate is subjected to the overall stress $\boldsymbol{\sigma}_0$ producing overall strain $\boldsymbol{\varepsilon}$.

As in the case of conventional composites, an effective interface between the matrix and the nanoparticles is considered [29], with a finite size which expresses the region surrounding the inclusions. The presence of many chains at the interphase means that much of the polymer is 'interphase like' [14]. Additionally, in intercalated nanocomposites, the polymer is

inserted into the clay structure between the layers in a crystallographically regular fashion. The degree of matrix–filler interaction becomes higher in the exfoliated composites, where the individual clay layers are separated and dispersed in the continuous polymer matrix.

Due to the above-mentioned reasons, for nanosized composites, the region around an inclusion is strongly interacted with the matrix material. Therefore, when the externally imposed stress field is high and plasticity occurs, the region involving the inclusions undergoes plastic deformation. So it is reasonable to assume that a plastic strain $\boldsymbol{\varepsilon}_{\mathrm{f}}^{\mathrm{p}}$ is related with the inclusion.

For low values of $\boldsymbol{\sigma}_0$ no plastic deformation is produced in both the inclusion and the matrix. As $\boldsymbol{\sigma}_0$ increases, plastic deformation will occur either in the matrix ($\boldsymbol{\varepsilon}^{\mathrm{p}}$) or in the inclusion region ($\boldsymbol{\varepsilon}_{\mathrm{f}}^{\mathrm{p}}$). The deformation then will become nonuniform, especially due to the presence of inclusions. The plastic parameters of the matrix are unknown and will be calculated from the constitutive description of the inclusions plastic deformation procedure. The quantities $\boldsymbol{\sigma}_0$, $\boldsymbol{\varepsilon}^{\mathrm{p}}$ and $\boldsymbol{\varepsilon}$ can be considered as the average values of the local quantities $\boldsymbol{\sigma}_{\mathrm{f}}$, $\boldsymbol{\varepsilon}_{\mathrm{f}}$, $\boldsymbol{\varepsilon}_{\mathrm{f}}^{\mathrm{p}}$ over all the randomly distributed single crystal grains (or inclusions).

To establish a relation between $\boldsymbol{\sigma}_{\mathrm{f}}$, $\boldsymbol{\varepsilon}_{\mathrm{f}}$, $\boldsymbol{\varepsilon}_{\mathrm{f}}^{\mathrm{p}}$ and $\boldsymbol{\sigma}_0$, $\boldsymbol{\varepsilon}$, $\boldsymbol{\varepsilon}^{\mathrm{p}}$ Kroner, Budiansky and Wu [19] assumed that the inclusion has a stress-free transformation strain equal to $\boldsymbol{\varepsilon}_{\mathrm{f}}^{\mathrm{p}} - \boldsymbol{\varepsilon}^{\mathrm{p}}$, and following Eshelby the strain inside it, due to the matrix-filler interaction, is given by:

$$\boldsymbol{\varepsilon}^{\mathrm{pt}} = \mathbf{S}\cdot(\boldsymbol{\varepsilon}_{\mathrm{f}}^{\mathrm{p}} - \boldsymbol{\varepsilon}^{\mathrm{p}}) \tag{15}$$

Eq. (15) expresses the difference between plastic deformation related with the inclusion and the matrix plastic deformation.

Following the procedure that is based on Chen and Cheng [18], and the Kroner and Budiansky model expressed by Eq. (15), the calculation of the stress $\boldsymbol{\sigma}_{\mathrm{f}}$ inside the filler, presented in detail in a previous work [23], results in the relation below:

$$\boldsymbol{\sigma}_{\mathrm{f}} = \mathbf{C}_{\mathrm{m}}\left[\mathbf{C}_{\mathrm{m}}^{-1}\cdot\boldsymbol{\sigma}_0 + (1-f_{\mathrm{p}})\beta(\boldsymbol{\varepsilon}_{\mathrm{f}}^{\mathrm{p}} - \boldsymbol{\varepsilon}^{\mathrm{p}}) + (f_{\mathrm{p}}-1)(\boldsymbol{\varepsilon}_{\mathrm{f}}^{\mathrm{p}} - \boldsymbol{\varepsilon}^{\mathrm{p}})\right] \tag{16}$$

or in its time derivative form:

$$\dot{\boldsymbol{\sigma}}_{\mathrm{f}} = \mathbf{C}_{\mathrm{m}}\left[\mathbf{C}_{\mathrm{m}}^{-1}\cdot\dot{\boldsymbol{\sigma}}_0 + (1-f_{\mathrm{p}})\beta\left(\dot{\boldsymbol{\varepsilon}}_{\mathrm{f}}^{\mathrm{p}} - \dot{\boldsymbol{\varepsilon}}^{\mathrm{p}}\right) + (f_{\mathrm{p}}-1)\left(\dot{\boldsymbol{\varepsilon}}_{\mathrm{f}}^{\mathrm{p}} - \dot{\boldsymbol{\varepsilon}}^{\mathrm{p}}\right)\right] \tag{17}$$

where $\beta = 2(4-5\nu)/(15(1-\nu))$, and ν is the Poisson ratio of the matrix.

Through the Kroner, Budiansky and Wu model a way is provided to transform the constitutive behaviour of single crystals into that of polycrystals and vice versa. In an analogous way Eq. (16) can be applied to formulate the elastoplastic behaviour of conventional and nanosized particulate composites. Eq. (16) bridges microstructural quantities such as $\boldsymbol{\sigma}_{\mathrm{f}}$, $\boldsymbol{\varepsilon}_{\mathrm{f}}^{\mathrm{p}}$, over macroscopic properties of the composite material.

5. Kinematics

5.1. Kinematics of composite's macrostructure

Given that the heterogeneous material examined behaves as a continuous isotropic one, when a stress field $\boldsymbol{\sigma}_0$ is imposed, an overall strain tensor $\boldsymbol{\varepsilon}_0$ and overall plastic strain tensor $\boldsymbol{\varepsilon}^{\mathrm{p}}$ are produced. The kinematic description developed by Rubin [21,22] that separates the elastic and plastic part will be applied in our analysis. This theory has been used to describe yielding of crystalline materials [21], as well as yielding of semicrystalline and amorphous polymers [30,31].

Following Rubin [21], in the case of uniaxial stress the components of the symmetric part of the tensor of plastic deformation rate are given by the following equations:

$$\begin{aligned} \mathrm{D}_{11}^{\mathrm{p}} &= \frac{\dot{I}_{\mathrm{p}}}{18}\left(\frac{a_{\mathrm{m}}^3-1}{a_{\mathrm{m}}^3}\right)\left(4a_{\mathrm{m}}^6+2\right) \\ \mathrm{D}_{22}^{\mathrm{p}} &= \mathrm{D}_{33}^{\mathrm{p}} = -\frac{\dot{I}_{\mathrm{p}}}{18}\left(\frac{a_{\mathrm{m}}^3-1}{a_{\mathrm{m}}^3}\right)\left(2a_{\mathrm{m}}^6+1\right) \end{aligned} \tag{18}$$

where a_{m} is the elastic stretch ratio and $\dot{I}_{\mathrm{p}}$ expresses the rate of plastic deformation, which has been modelled in previous work [31] and is expressed, in terms of a distribution density function as follows:

$$\dot{I}_{\mathrm{p}} = \frac{\dot{a}}{a(a_{\mathrm{m}}^{\mathrm{y}}-1)s\sqrt{2\pi}}\int_1^a \exp\left[-\frac{1}{2}\left(\frac{a_i-\mu}{s}\right)^2\right]\mathrm{d}a_i \tag{19}$$

where $\dot{a}$ is the imposed strain rate, μ and s are the mean value and the standard deviation of the distribution and $a_{\mathrm{m}}^{\mathrm{y}}$ is the yield stretch ratio.

5.2. Kinematics of effective particle microstructure

On the other hand, in order to apply constitutive Eq. (16), the plastic deformation tensor $\boldsymbol{\varepsilon}_{\mathrm{f}}^{\mathrm{p}}$ related with the fillers must also be calculated. In this case, the kinematic description introduced by Rubin for small strains will be applied. Following Rubin's theory which is analytically presented in previous works [21,30,31], the flow rule which determines the rate of the symmetric part of plastic deformation tensor is given by the expression:

$$\mathbf{D}_{\mathrm{f}}^{\mathrm{p}} = \dot{\gamma}\tilde{\mathbf{D}}_{\mathrm{f}}^{\mathrm{p}} \tag{20}$$

where $\dot{\gamma}$ is a non-negative function which will be specified in the sequel and $\tilde{\mathbf{D}}_{\mathrm{f}}^{\mathrm{p}}$ defines the directions of the plastic velocity gradient tensor. These directions are based on the dyadic $\mathbf{m}_{\mathrm{i}}\otimes\mathbf{m}_{\mathrm{j}}$, where $\mathbf{m}_{\mathrm{i}}$, $\mathbf{m}_{\mathrm{j}}$ are linearly independent unitless vectors that play the role of microstructural variables, and for a two-dimensional problem they are given by the relations: $\mathbf{m}_1 = (1+\boldsymbol{\varepsilon}_{11}^{\mathrm{f}})\mathbf{a}_1$, $\mathbf{m}_2 = (1+\boldsymbol{\varepsilon}_{11}^{\mathrm{f}})\mathbf{a}_2$, where $\mathbf{a}_1$ and $\mathbf{a}_2$ are the orthonormal vectors $\mathbf{a}_1=\{1,0\}$, $\mathbf{a}_2=\{0,1\}$. Consequently tensor $\tilde{\mathbf{D}}_{\mathrm{f}}^{\mathrm{p}}$ will be given by the following equation [22]:

$$\tilde{\mathbf{D}}_{\mathrm{f}}^{\mathrm{p}} = [\boldsymbol{\sigma}_{\mathrm{f}}' \cdot (\mathbf{m}_1' \otimes \mathbf{m}_1')]\left(\mathbf{m}_1' \otimes \mathbf{m}_1' - \frac{1}{3} m_{11}' \mathrm{I}\right) \Big/ \tau + [\boldsymbol{\sigma}_{\mathrm{f}}' \cdot (\mathbf{m}_2' \otimes \mathbf{m}_2')]\left(\mathbf{m}_2' \otimes \mathbf{m}_2' - \frac{1}{3} m_{22}' \mathrm{I}\right) \Big/ \tau + [\boldsymbol{\sigma}_{\mathrm{f}}' \cdot (\mathbf{m}_1' \otimes \mathbf{m}_2')]\left(\mathbf{m}_1' \otimes \mathbf{m}_2' + \mathbf{m}_2' \otimes \mathbf{m}_1' - \frac{2}{3} m_{12}' \mathbf{I}\right) \Big/ \tau \tag{21}$$

where $\boldsymbol{\sigma}_{\mathrm{f}}'$ is the deviatoric stress tensor related with the inclusion. The quantities $\mathbf{m}_{\mathrm{i}}'$ are given by $\mathbf{m}_{\mathrm{i}}' = \mathbf{m}_{\mathrm{i}}/\det m_{\mathrm{ij}}$ where metric m_{ij} is defined as: $m_{\mathrm{ij}} = \mathbf{m}_{\mathrm{i}} \cdot \mathbf{m}_{\mathrm{j}}$. Every term in Eq. (21) is divided by τ which is the maximum shear stress, denoting that yield mainly occurs in the direction of this shear stress.

Then Eqs. (20) and (21) give:

$$\begin{aligned} \mathrm{D}_{\mathrm{f}_{11}}^{\mathrm{p}} &= \dot{\gamma}_{11} \tilde{\mathrm{D}}_{\mathrm{f}_{11}}^{\mathrm{p}} \\ \mathrm{D}_{\mathrm{f}_{22}}^{\mathrm{p}} &= \dot{\gamma}_{22} \tilde{\mathrm{D}}_{\mathrm{f}_{22}}^{\mathrm{p}} \end{aligned} \tag{22}$$

Hardening laws introduced for polycrystalline materials by Khan [32], are also applied here and $\dot{\gamma}_{11}$ and $\dot{\gamma}_{22}$ will be expressed as follows:

$$\begin{aligned} \dot{\gamma}_{11} &= \frac{(\dot{\sigma}_{\mathrm{f}_{11}})^n}{h} \\ \dot{\gamma}_{22} &= \frac{(\dot{\sigma}_{\mathrm{f}_{22}})^n}{h} \end{aligned} \tag{23}$$

where $\dot{\sigma}_{\mathrm{f}_{11}}$, and $\dot{\sigma}_{\mathrm{f}_{22}}$ are the corresponding components of tensor $\dot{\boldsymbol{\sigma}}_{\mathrm{f}}$ expressed by Eq. (17), n is an exponent and h is the hardening modulus, treated both as material parameters.

6. Simulation of tensile results of polymer/clay nanocomposites

The calculations were made using the software Mathematica [33] for numerical integration of the corresponding equations, in the following way.

Assuming a two-dimensional problem, two parallel numerical calculations were performed, that concern both the composite material as a whole and the effective particle plastic deformation. Combination of Eqs. (21)–(23) led to the calculation of $\mathrm{D}_{\mathrm{f}_{11}}^{\mathrm{p}}$, and $\mathrm{D}_{\mathrm{f}_{22}}^{\mathrm{p}}$, and consequently the determination of the two components of effective particle plastic deformation tensor $\boldsymbol{\varepsilon}_{\mathrm{f}}^{\mathrm{p}}$, namely $\varepsilon_{\mathrm{f}_{11}}^{\mathrm{p}}$, $\varepsilon_{\mathrm{f}_{22}}^{\mathrm{p}}$. The integration has been made numerically using small time steps, until a high convergence has been obtained. Due to the assumption of the isotropic nature of particulates and the type of testing, the other components are taken equal to zero. Regarding the composite material, which is also an isotropic one, the formulation used in the previous work by Kontou [23] for the elastic stretch ratio a_{m}, together with Eqs. (18) and (19) were utilized to calculate the components of plastic deformation tensor $\mathrm{D}_{11}^{\mathrm{p}}$, $\mathrm{D}_{22}^{\mathrm{p}}$. Through them the two components of the corresponding strain tensor $\boldsymbol{\varepsilon}^{\mathrm{p}}$ could be evaluated. Finally, the overall stress $\boldsymbol{\sigma}_0$ of the composite was calculated through the total volumetric average strain $\boldsymbol{\varepsilon}^{\mathrm{T}}$ introduced by Chen et al. [18]. Since in their work it was assumed that $\boldsymbol{\sigma}_0 = \mathbf{C}^* \cdot \boldsymbol{\varepsilon}^{\mathrm{T}}$, where

$$\boldsymbol{\varepsilon}^{\mathrm{T}} = \boldsymbol{\varepsilon}_0 + f_{\mathrm{p}}(\boldsymbol{\varepsilon}_{\mathrm{f}}^{\mathrm{p}} - \boldsymbol{\varepsilon}^{\mathrm{p}}) \tag{24}$$

it is extracted that

$$\boldsymbol{\sigma}_0 = \mathbf{C}^* \cdot \left[\boldsymbol{\varepsilon}_0 + f_{\mathrm{p}}(\boldsymbol{\varepsilon}_{\mathrm{f}}^{\mathrm{p}} - \boldsymbol{\varepsilon}^{\mathrm{p}})\right] \tag{25}$$

In the case of the pure matrix the following expression after Rubin [22] has been used:

$$\sigma_{\mathrm{matrix}} = \mu\left(J_{\mathrm{m}}^{-1}\frac{a_{\mathrm{m}}^3 - 1}{a_{\mathrm{m}}}\right) \tag{26}$$

where $J_{\mathrm{m}} = 1 + (\mu/3K)((a_{\mathrm{m}}^3 - 1)/a_{\mathrm{m}})$, μ is the Lamé constant of tensor $\mathbf{C}_{\mathrm{m}}$ and K is the matrix bulk modulus.

By introducing all the above-mentioned quantities in constitutive Eq. (17), the tensile stress for all material types was obtained and plotted versus total strain.

For the calculations, the Poisson ratio of the matrix was equal to 0.35 and for nanocomposites 0.25. The only unknown parameters are the distribution function constants μ and s of Eq. (19), as well as the hardening modulus h. For series A the mean value was fitted equal to 0.0038 for the matrix and 0.0031 for the nanocomposites, whereas for series B these values were 0.0091 and 0.0031, respectively. The standard deviation s was always equal to the half of the mean value. The hardening modulus was fitted to be the same in two directions and equal to 10 GPa. Exponent n of Eq. (23) was fitted equal to 0.1.

The calculations were carried out in the following way: for each sample, according to Table 1 the corresponding set of parameters, i.e., aspect ratio, modulus and volume fraction of the effective particle were introduced in the Taya and Chou model Eq. (1) to generate the theoretical curves of Figs. 1 and 2. Thereafter, they were used to compute the effective particle stiffness tensor, $\mathbf{C}_{\mathrm{f}}$ and through $\mathbf{C}_{\mathrm{f}}$ and $\mathbf{C}_{\mathrm{m}}$ the effective elastic moduli tensor $\mathbf{C}^*$ from Eq. (13). Finally, as noted before, these quantities were inserted in constitutive Eq. (17).

The simulated results are shown in Figs. 3 and 4 for both sets of experiments. From these plots a good prediction between experimental data and theoretical results is observed, and the

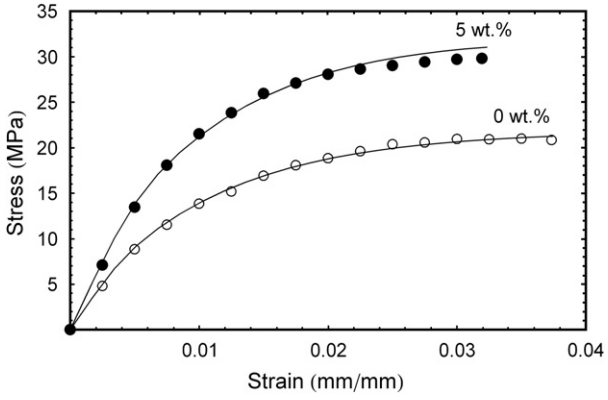

Fig. 3. Tensile stress–strain results of pure Dow epoxy resin (series A) and its nanocomposite with 5 wt% clay concentration ($f_{\mathrm{p}} = 0.0978$). Points: experimental data after Luo and Daniel [15]. Lines: simulated results.

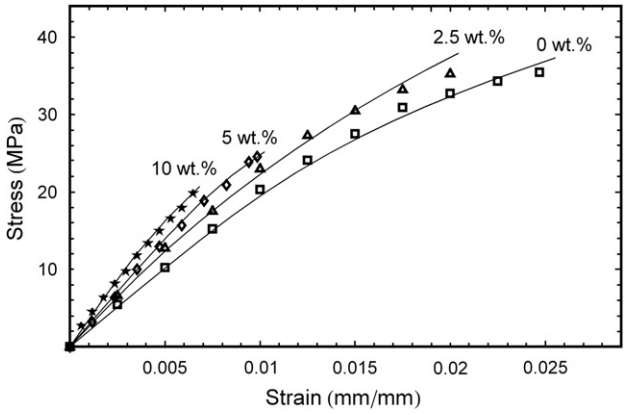

Fig. 4. Tensile stress–strain results of the neat three component Ciba–Geigy epoxy system (series B) and its nanocomposites with 2.5 ($f_p = 0.0255$), 5 ($f_p = 0.0978$) and 10 ($f_p = 0.1955$) wt% concentration of clay. Points: experimental data after Daniel et al. [24]. Lines: simulated results.

selected values of hardening moduli related with the inclusions plastic deformations can successfully describe the hardening behaviour of the overall composite material. Thus, the foregoing analysis reveals that the proposed model manages to reproduce satisfactorily the experimental data of Daniel et al. [24] for 5 and 10 wt%, where the values of $d_{(001)}$ are clearly specified or expected to lie in a certain range, as well as for clay concentration of 2.5 wt% where the authors did not provide any measurement for $d_{(001)}$ (as already stated in Section 3). The best fit of the experimental data for this nanocomposite was achieved for $d_{(001)}$=2.4 nm and it is shown in Fig. 4.

7. Conclusions

In this work, a model was presented to formulate the elastoplastic response of particulate composite materials, experimentally tested elsewhere. The model based on Mori–Tanaka theory, for the estimation of the elastic stiffness tensor for the composite materials, is combined with the self-consistent model of Budiansky and Wu, valid for crystal plasticity, under the basic assumption of the development of plastic strain in the inclusion region. This assumption is reasonable for nanostructured materials by virtue of the strong interaction of the region around the inclusion with the matrix. In order to make reliable predictions, the modelling strategy has to take into account the intrinsically hierarchical morphology of intercalated nanoclay, as well as the morphology of the surrounding matrix. This formalism enables correlation of the macroscopic plastic response of heterogeneous materials with their microstructural parameters. The effects of incomplete intercalation and partial exfoliation are examined by treating the intercalated nanoclay as a homogeneous 'effective particle'. The model was proved to successfully describe the tensile response of epoxy/clay nanocomposites for different strain rates, performed elsewhere. Back-analysis of the experimental data for clay concentration 2.5 wt% provided an estimate for the interlayer spacing around 2.4 nm for this nanocomposite, which could not be detected by TEM or XRD techniques.

Acknowledgements

This work has been funded by the project PENED 2003. The project is co-financed 75% of public expenditure through EC – European Social Fund, 25% of public expenditure through Ministry of Development – General Secretariat of Research and Technology and through private sector, under measure 8.3 of OPERATIONAL PROGRAMME "COMPETITIVENESS" in the 3rd Community Support Programme.

References

[1] Komarneni S. Nanocomposites. J Mater Chem 1992;2(12):1219–30.
[2] Giannelis EP. Polymer layered silicate nanocomposites. Adv Mater 1996;8(1):29–35.
[3] Usuki A, Kojima Y, Kawasumi M, Okada A, Fukushima Y, Kurauchi T, et al. Synthesis of nylon 6-clay hybrid. J Mater Res 1993;8:1179–83.
[4] Kojima Y, Usuki A, Kawasumi M, Okada A, Fukushima Y, Kurauchi T, et al. Mechanical properties of nylon 6-clay hybrid. J Mater Res 1993;8:1185–9.
[5] Yano K, Usuki A, Okada A, Kurauchi T, Kamigaito O. Synthesis and properties of polyimide–clay hybrid. J Polym Sci Part A Polym Chem 1993;31:2493–8.
[6] Sinha Ray S, Okamoto M. Polymer/layered silicate nanocomposites: a review from preparation to processing. Prog Polym Sci 2003;28: 1539–641.
[7] Biswas M, Sinha Ray S. Recent progress in synthesis and evaluation of polymer–montmorillonite nanocomposites. Adv Polym Sci 2001;155: 167–221.
[8] Maksimov RD, Gaidukovs S, Kalnins M, Zicans J, Plume E. A nanocomposite based on a styrene-acrylate copolymer and native montmorillonite clay 1. Preparation, testing, and properties. Mech Compos Mater 2006;42(1):45–54.
[9] Hui CY, Shia D. Simple formulas for the effective moduli of unidirectional aligned composites. Polym Eng Sci 1998;38(5):774–82.
[10] Shia D, Hui CY, Burnside SD, Giannelis EP. An interface model for the prediction of Young's modulus of layered silicate-elastomer nanocomposites. Polym Compos 1998;19(5):608–17.
[11] Osman MA, Rupp JEP, Suter UW. Tensile properties of polyethylene-layered silicate nanocomposites. Polymer 2005;46(5):1653–60.
[12] Guth E. Theory of filler reinforcement. J Appl Phys 1945;16(1):20–5.
[13] Kerner EH. The elastic and thermo-elastic properties of composite media. Proc Phys Soc 1956;B69(8):808–13.
[14] Brune DA, Bicerano J. Micromechanics of nanocomposites: comparison of tensile and compressive elastic moduli, and prediction of effects of incomplete exfoliation and imperfect alignment on modulus. Polymer 2002;43:369–87.
[15] Luo J-J, Daniel IM. Characterization and modeling of mechanical behavior of polymer/clay nanocomposites. Compos Sci Technol 2003; 63:1607–16.
[16] Eshelby JD. The determination of the elastic field of an ellipsoidal inclusion and related problems. Proc R Soc London 1957;A241:376–96.
[17] Mori T, Tanaka K. Average stress in matrix and average elastic energy of materials with misfitting inclusions. Acta Metall 1973;21(5):571–4.
[18] Chen C-H, Cheng C-H. Effective elastic moduli of misoriented short-fiber composites. Int J Solids Structures 1996;33(17):2519–39.
[19] Budiansky B, Wu TY. Theoretical prediction of plastic strains of polycrystals. In: Proceedings of the 4th US National Congress of Applied Mechanics; 1962. p. 1175–85.
[20] Taya M, Chou T-W. On two kinds of ellipsoidal inhomogeneities in an infinite elastic body: an application to a hybrid composite. Int J Solids Structures 1981;17:553–63.
[21] Rubin MB. Plasticity theory formulated in terms of physically based microstructural variables–Part I. Theory. Int J Solids Structures 1994;31(19):2615–34.

[22] Rubin MB. Plasticity theory formulated in terms of physically based microstructural variables—Part II. Examples. Int J Solids Structures 1994;31(19):2635–52.
[23] Kontou E. Micromechanics model for particulate composites. Mech Mater 2007;39:702–9.
[24] Daniel IM, Miyagawa H, Gdoutos EE, Luo J-J. Processing and characterization of epoxy/clay nanocomposites. Exp Mech 2003;43(3):348–54.
[25] Taya M, Mura T. On stiffness and strength of an aligned short-fiber reinforced composite under uniaxial applied stress when the composite contains fiber-end cracks. J Appl Mech 1981;48:361.
[26] Sheng N, Boyce MC, Parks DM, Rutledge GC, Abes JI, Cohen RE. Multiscale micromechanical modeling of polymer/clay nanocomposites and the effective clay particle. Polymer 2004;45:487–506.
[27] Manevitch OL, Rutledge GC. Elastic properties of a single lamella of montmorillonite by molecular dynamics simulation. J Phys Chem B 2004;108:1428–35.
[28] Kint DPR, Seeley G, Gio-Batta M, Burgess AN. Structure and properties of epoxy-based layered silicate nanocomposites. J Macromol Sci Part B Phys 2005;44:1021–40.
[29] Odegard GM, Clancy TC, Gates TS. Modeling of the mechanical properties of nanoparticle/polymer composites. Polymer 2005;46: 553–62.
[30] Spathis G, Kontou E. Experimental and theoretical description of the plastic behaviour of semicrystalline polymers. Polymer 1998;39(1): 135–42.
[31] Spathis G, Kontou E. Mechanism of plastic deformation for polycarbonate under compression by a laser extensometer technique. J Appl Polym Sci 2001;79(14):2534–42.
[32] Khan AS, Huang S. Continuum theory of plasticity. New York: John Wiley and Sons; 1995.
[33] Wolfram S. Mathematica, a system for doing mathematics by computer. 4th ed. New York: Wolfram Research Inc; 1999.